This article has been accepted for publication in IEEE Transactions on Mobile Computing. This is the author's version which has not been fully edited and content may change prior to final publication. Citation information: DOI 10.1109/TMC.2024.3397164

Mobility-Aware Congestion Control for Multipath QUIC in Integrated Terrestrial Satellite Networks

Wenjun Yang, *Graduate Student Member, IEEE,* Lin Cai, *Fellow, IEEE,* Shengjie Shu, and Jianping Pan, *Fellow, IEEE*

Abstract—The Integrated Terrestrial and LEO Satellite Network (ITSN) has a high bandwidth-delay product (BDP) and high-speed movement, which makes congestion control difficult. We develop a Mobility-Aware COngestion control (MACO) algorithm for multipath QUIC (MPQUIC) in ITSN. MACO models the dynamic interactions between MPQUIC subflows and LEO networks, including handovers and outages triggered by satellite movement, and changes in network topology and link conditions. With the knowledge of network dynamics influenced by mobility, MACO can estimate changes in path BDP without solely relying on lengthy network probing. It employs a quick start (QS) and an effective congestion avoidance (CA) mechanism based on a multipath fluid model. The QS sets an appropriate initial cwnd to shorten the slow start duration. The CA applies a square root function to quickly increase the cwnd to the equilibrium and conservatively increase when approaching the BDP. We conduct a series of experiments to evaluate MACO using network simulator 3 (ns-3) based on collected data traces on Starlink. Simulation results demonstrate that MACO can achieve upto three times higher throughput and improve the convergence performance by 70.67% against benchmark algorithms.

Index Terms—MPQUIC, congestion control, mobility management, satellite network, BDP

1 Introduction

Next-generation wireless networks (6G) are increasingly embracing the Integrated Terrestrial and Low Earth Orbit (LEO) Satellite Networks (ITSN) for ubiquitous coverage [1]–[4]. Walker-type constellation in Fig. 1 has been adopted in LEO networks, e.g., the Starlink developed by SpaceX, which comprises satellites that are uniformly distributed in orbits with the same orbit inclination and altitude.

One typical challenge in ITSN is raised by the satellite movement [5]. Satellite moving is of high speed, so the handover between users and access satellites will be frequent, leading to severe connection interruptions.

According to [6], [7], multipath transport protocols, such as multipath TCP (MPTCP) [8] and multipath QUIC (MPQUIC) [9] have a great potential to support seamless connectivity migration during handover. Compared to MPTCP, MPQUIC is more desirable in mobile environments for two reasons: First, MPQUIC spends 1 RTT to initialize a subflow if the subflow has never been established before, or 0 RTT otherwise. In the event of a handover failure, MPQUIC consumes 0 RTT to restore the disconnected subflow. Furthermore, each MPQUIC connection is associated with a 64-bit connection ID (CID) instead of a four-tuple set [10]. Thus even if the address and/or port are changed due to mobility, the connection remains active.

However, the existing congestion control algorithms for MPQUIC in ITSN are undesirable. They can be classified into four categories: loss-based [12]–[14], delay-based [15], [16], bandwidth-delay product (BDP) based [17], and learning-based [18], [19].

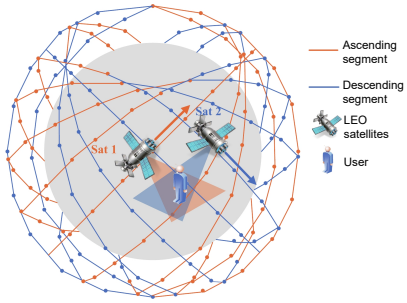

Fig. 1. Walker-type satellite constellation [11].

In ITSN, packet loss can occur due to various factors such as handover loss or transmission error caused by atmospheric conditions, while high delay variations can result from routing path detours when certain satellites become unreachable during satellite movement. Therefore, relying solely on packet loss or delay signals is insufficient to accurately identify congestion levels in LEO networks. BDP-based solutions state that the BDP serves as a critical indicator of congestion levels, so obtaining BDP information is a fundamental step. However, they necessitate at least one RTT to probe network conditions to figure out the BDP information. As ITSN has a relatively long propagation delay, using one RTT to do network probing is expensive. Learning-based solutions also suffer from low efficiency at the initial stage because they cannot obtain sufficient data to predict network conditions at the beginning.

Motivated by the above critical issues, our goal is to leverage mobility information in congestion control and to better trade off performance metrics including through-

• *W. Yang and L. Cai are with the Department of Electrical and Computer Engineering, University of Victoria, Victoria, BC V8P 5C2, Canada. S. Shu and J. Pan are with the Department of Computer Science, University of Victoria, Victoria, BC V8P 5C2, Canada.*
E-mail: {wenjunyang, shengjies, pan}@uvic.ca, cai@ece.uvic.ca

put, responsiveness, and TCP friendliness. To achieve this, we present a novel Mobility-Aware COngestion control (MACO) algorithm for MPQUIC in ITSN. In addition to the preliminary results presented in [10], this study aims to tackle more complex scenarios when the bottleneck arises in various locations, including ground-to-satellite access links, inter-satellite links and core networks. The main contributions and novelties of this paper are three-fold.

First, we propose an efficient BDP estimation approach in the ITSN mobile scenario instead of solely relying on lengthy network probing.

1) To derive the bottleneck bandwidth, we take advantage of the regularity of satellite motion to predict the access link condition changes (Section 4.1.1), and also employ the Adaptive Kalman Filter (AKF) to swiftly offset the estimation errors in cases where the bottleneck arises from non-satellite networks (Section 4.1.2).
2) In the process of delay estimation, we leverage the knowledge of the changing distance between ground users and satellites and statistical analysis of the delay distribution based on measurements spanning one year over Starlink satellites (Section 4.1.3).

Second, we present the MACO algorithm which has two components: BDP-inspired quick start and mobility-aware congestion avoidance.

1) In the quick start phase, MACO sets the initial congestion window (cwnd) to a large yet safe value based on the estimated path BDP as well as learning from history settings across different subflows (Section 4.2).
2) In the congestion avoidance design, MACO utilizes a multipath fluid model and the square root function to trade off performance metrics including throughput, convergence, and TCP friendliness. This approach ensures aggressive cwnd growth when the current cwnd is far below the estimated BDP and conservative growth when approaching it, thereby effectively exploring network capacity (Section 5.2).

Finally, based on an MPQUIC prototype we developed [20], we implement the MACO and benchmark algorithms. Extensive evaluation results demonstrate that:

1) MACO is more adaptive to dynamics such that its cwnd can reach up to the peak BDP, that is, 300 MSS (maximum segment size), which is 20% and 200% higher than that of BBR [21] and OLIA [12], respectively.
2) Compared to benchmarks, MACO improves the throughput by three times without causing a longer queuing delay.
3) While ensuring TCP friendliness, MACO takes 70.67% less time to recover to the network capacity when packet loss occurs compared to OLIA.

The rest of this paper is organized as follows. Section 2 summarizes the related works. Section 3 presents the system model and the problems to address. Section 4 elaborates how quick start selects the appropriate slow start threshold and initial cwnd for efficient network probing. Section 5 elaborates on the detailed design of the congestion avoidance algorithm. To verify the performance gain of our proposal, experiments using ns-3 along with detailed analyses are given in Section 6, followed by concluding remarks and further research issues in Section 7.

2 Related Work

In this section, recent studies on ITSN networks are reviewed, including existing mobility management, MPQUIC-based solutions, and congestion control mechanisms. Table 1 summarizes the salient features of the existing studies.

2.1 Mobility Management

To overcome the mobility issue that stems from the conventional TCP/IP stack in terrestrial networks, new architecture design paradigms have been suggested by the research community. They can be categorized into two schools: 1) clean-slate architectures, e.g., MobilityFirst [22], Named Data Networking (NDN) [23], RINA [24], Content-Centric Networking (CCN) [25], and Data-Oriented Network Architecture (DONA) [26]; 2) evolutionary architectures, e.g., Locator/ID separation protocol (LISP) [27], New IP [28], and Trotsky [29].

The above solutions share a common design rationale that a cleaner separation of identity and location is instrumental to enhancing endpoint mobility. However, the network sides (i.e., satellites) rather than endpoints dominate the mobility and handover issues in the ITSN scenario. As a result, satellite-mobility-driven approaches, such as NDM [5], MSN [30], and QIH [31] are newly developed. They focus on the handover prediction by considering the movement of both user terminals and satellites, followed by a handover-aware protocol design. However, they establish a single TCP connection over terrestrial and space networks, leading to two problems. First, the single connection runs in a break-before-make fashion to deal with the handover, referred to as hard handover, it has the momentary connection breakage issue [43]. Second, the TCP connection has to be re-established with new parameters (another three-way handshake) during a session if the client changes its IP address, which is prohibitive in ITSN cases where the RTT is generally far higher than the counterpart in terrestrial networks.

2.2 Multipath-enabled Transport Protocols

Given the frequent handover in mobile networks, multipath-enabled transport protocol design is more promising. There have been several multipath transport protocols such as DCCP [44], CMT-SCTP [45], MPTCP [8], and MPQUIC [9].

DCCP was mainly invented for mobility support because it is useful for connection migration thanks to the multihoming feature. However, it does not support concurrent multipath transmission, thereby motivating the development of CMT-SCTP. CMT-SCTP has largely improved the throughput by using multiple paths to transmit data simultaneously. However, CMT-SCTP is an extension of SCTP, which has limited deployment compared to more widely adopted protocols such as TCP and UDP. Thus, researchers shift their interests to MPTCP and MPQUIC.

MPQUIC, the latest proposal, has inherited the advantages of both CMT-SCTP and MPTCP, demonstrating great potential in various scenarios including ITSN [10], [35], [46]. First of all, MPQUIC is robust to the connection migration caused by mobility because each QUIC connection

TABLE 1
Summary of existing solutions

Properties	Clean-slate Architecture	Backward Compatible	Network Mobility	Soft Handover	QoS Guarantee	SS Design
Algorithms	MobilityFirst [22], NDN [23], RINA [24], CCN [25], and DONA [26]	LISP [27], New IP [28], and Trotsky [29]	NDM [5], MSN [30], and QIH [31]	OLAPS [32], GADaM [33], HBES [34], and MPDTP [35]	MPDTP [35]	[36], and HPCC [37]
Properties	CA Design	Reactive	Proactive	Learning-based	Model-based	Loss-based
Algorithms	DCQCN [38], TIMELY [39], HPCC [37], ExpressPass [40], NDP [41], Homa [42], BBR [21], and OLIA [12]	DCQCN [38], TIMELY [39], and HPCC [37]	ExpressPass [40], NDP [41], and Homa [42]	OLAPS [32], GADaM [33], HBES [34], and HPCC [37]	MPDTP [35], and BBR [21]	OLIA [12]

is identified with a Connection ID (CID) which can be associated with multiple IP addresses. In addition, different from MPTCP which needs the three-way handshake to establish or restore a connection, MPQUIC takes only 1 RTT to initialize a subflow, or 0 RTT to restore it. This feature is preferable in mobile scenarios. MPQUIC also maintains a global view about the status of each path through a 'PATHS' frame, e.g., whether the path is active, underperforming, or broken. These statistics can be used to speed up the handover process in mobility scenarios [9].

Recent works, such as OLAPS [32], GADaM [33], HBES [34], and MPDTP [35], have explored the usage of multi-path transport protocols in mobile scenarios. OLAPS and GADaM utilize learning models to gain a better understanding of network dynamics in mobile scenarios, and then design an optimal path scheduling policy. HBES mainly aims to mitigate the HoL Blocking issues in the presence of mobility, thus improving the quality of experience (QoE) perceived by the receiver. MPDTP focuses on the deadline guarantee by taking into account challenges in the ITSN scenario, such as high loss rate, limited bandwidth, and long round trip time (RTT).

2.3 Congestion Control Algorithms

Satellite networks are featured by high bandwidth and long delays. For the traditional TCP/IP stack, at the beginning of a new connection, the sender executes a slow start to probe the usable bandwidth along the path [47], taking a few RTTs, which is not desirable for small file transfer. Authors in [36], [37] argued that the initial window should be set to a larger value against the original value which is typically 1 MSS.

TCP uses a congestion window to explore available bandwidth, which is adjusted in an additive increasing and multiplicative decreasing (AIMD) fashion [48]. The AIMD can ensure a reasonably fair share of bandwidth but can be slow in mobile environments where the channel quality changes fast due to fading, shadowing, and handover [49].

The latest efforts at congestion avoidance can be generally divided into two directions: reactive and proactive congestion control. DCQCN [38], TIMELY [39], and HPCC [37] are the reactive ones, which investigated novel congestion signals to detect congestion. The proactive approaches, e.g., ExpressPass [40], NDP [41], and Homa [42] integrated priority scheduling policies with congestion control to schedule packets for the purpose of congestion-free, but they are unable to get the required information and take action in the first RTT.

In 2016, BBR [21] was proposed as model-based congestion control, which skips the concept of cwnd. It measures bottleneck bandwidth and RTT to control the sending rate directly. It appears to be a great improvement especially when it works with QUIC [50]. However, BBR with multi-path support is not yet available as the coupled design of the pacing gain rate for multiple paths remains an open issue. Therefore, MPQUIC has opted for OLIA [12] as the standard congestion control scheme which is loss-based. However, OLIA cannot translate the packet loss accurately in ITSN and incurs performance degradation.

Therefore, in this paper, we propose the MPQUIC-supported ITSN architecture where MPQUIC deals with smooth handover and fast connection establishment. In addition, we emphasize the importance of collaboration between the end-system and network side, enabling the MPQUIC to be aware of mobility events, and thus it can make a wise and effective decision on congestion control to adapt to the dynamic link capacity.

3 System Model and Problem Statement

In this section, we first model the behavior of MPQUIC subflows under the impact of LEO satellite movements and then identify the problems when applying existing congestion control algorithms to MPQUIC in the ITSN scenario.

3.1 System Model

We consider the Walker-type satellite constellation. As of now, most satellite networks operate on a bent pipe principle, which means satellites are used to relay information. Data is transmitted to the satellite, which sends it right back down to the nearest ground station [51], [52], so we focus on this scenario as shown in Fig. 2. The main notations used throughout this paper are listed in Table 2.

Fig. 2 depicts the ITSN system, consisting of the MPQUIC-capable end hosts H_1 and H_2, the LEO satellites G_1–G_3 in the same orbit plane, and ground station E_1. Assuming all satellites move from south to north at velocity v over time, and H_1 is directly connected to G_1, G_2, G_3, etc. The distance between two adjacent satellites in the same orbit is denoted by R_1, while R_2 represents the radius of the satellite footprint.

At time t_1, H_1 is in the footprint of satellite G_1 by which the first MPQUIC subflow denoted by F_0 is created. In the presence of satellite movement, H_1 enters into the handover (HO) area after a while, in which the HO area refers to the

TABLE 2
The main notations and definitions

Notation	Definition
H_1, H_2	A pair of the sender and the receiver.
G_1–G_3	LEO satellites.
E_1	Ground station.
d_1	Distance traveled by H_1 across the HO area.
d_2	Distance between two adjacent HO areas.
R_1	Distance between two adjacent satellites.
R_2	Radius of the satellite footprint.
w_r	The cwnd of path r.
τ_r	The RTT of path r.
x_r	Transmission rate over path r.
$\Omega_r(t)$	Initial value of cwnd.
$\mathcal{B}_r(t)$	Instantaneous path BDP.
$\overline{\mathcal{B}_r}(t)$	Averaged path BDP over an interval τ_r.
$\mathcal{C}_{r,t}$	Bottleneck bandwidth over path r at time t.
$\mathcal{C}^A_{r,t}$	Bandwidth of ground-satellite links.
$\mathcal{C}^N_{r,t}$	Bandwidth of core networks.
$\mathcal{D}_{r,t}$	Round-trip propagation delay.
$\mathcal{W}_r$	Set of all cwnd when congestion occurs.

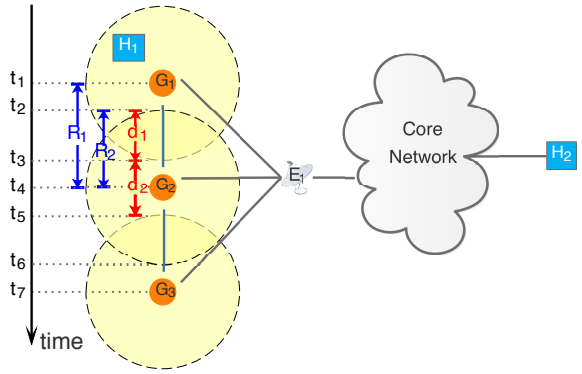

Fig. 2. MPQUIC-supported ITSN network architecture.

area where the footprint of two adjacent satellites overlaps. Within the HO area, H_1 can create a new subflow F_1 by attaching its second interface to the reachable satellite. Denote by d_1 the distance traveled from the point at which $H1$ enters the HO area to the point at which it exits. When H_1 moves out of the HO area, we assume that the northernmost satellite becomes unreachable and the associated connection has to be migrated to a new coming satellite. For example, at the time t_3 when H_1 approaches to edge of the footprint of G_1, we assume that the received signal strength (RSS) of the interface associated with F_0 is below a threshold, which triggers service outage and MPQUIC immediately migrates the connection of F_0 seamlessly by attaching to the available satellite G_2 while maintaining the connection continuity of F_1. As time goes by, H_1 will re-enter and leave the new HO area periodically. d_2 is the distance between the current HO area and the subsequent one.

3.2 Problem Statement

To investigate the problem, we first give the discrete-time topology states as shown in Fig. 3. The network topology undergoes periodic changes. Except for state s_1 where only one subflow is established at the beginning, two subflows between H_1 and H_2 are created in subsequent states. In state s_2, as H_1 enters the HO area, the two subflows connect to

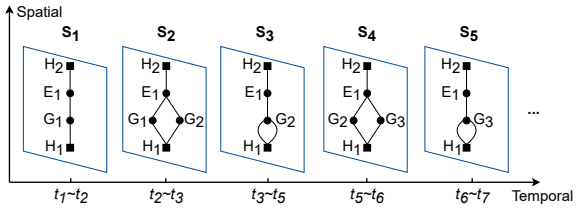

Fig. 3. A topological breakdown over time.

two different satellites. In state s_3, when H_1 moves to an area where only one satellite is visible, both subflows connect to the same satellite. This cyclic pattern of connectivity switching is a characteristic of the network topology in this scenario.

OLIA [12] has been widely adopted as a multipath-based congestion control algorithm for MPTCP and MPQUIC. Let $\mathcal{R}$ be the set of available paths, and w_r and τ_r are the current cwnd and RTT of path $r \in \mathcal{R}$, respectively. The behavior of OLIA during the congestion avoidance (CA) phase is summarized below:

- For each ACK on path r, increase w_r by:

$$\frac{w_r/\tau_r^2}{\left(\sum_{p\in\mathcal{R}} w_p/\tau_p\right)^2} + \frac{\alpha_r}{w_r} \tag{1}$$

  where α_r is to guarantee the responsiveness of OLIA. By measuring the current RTT and the number of transmitted bits since the last loss, it determines whether a path is the best path or not. Then α_r is positive for all best paths with a small window and negative for paths that are not the best path while having a maximum window, and it is zero for the path that already has the maximum window.
- For each loss on path r, decrease w_r by $\frac{w_r}{2}$.

For ITSN with large BDP and periodical topological changes, OLIA encounters the following issues.

Bandwidth underutilization: OLIA suffers from bandwidth underutilization given its slow-start probing strategy when initializing new subflows in states s_1 and s_2. The time required by the slow start (SS) to reach a bit rate $\mathcal{C}$ is

$$t_{\text{SS}} = \tau \cdot \left(1 + \log_2 \frac{\mathcal{C}\cdot\tau}{l\cdot\Omega}\right),$$

where l is the average packet length expressed in bits, and Ω represents the initial cwnd. For instance, given that $\mathcal{C} = 200$ Mbps, $\tau = 100$ ms, $l = 1$ KB, and $\Omega = 1$ MSS, we have $t_{\text{SS}} = 1.13$ seconds which is too slow. In addition, upon the reception of a packet loss signal, OLIA will decrease cwnd by half and switch to the CA phase, and increase cwnd additively as in (1) to probe for the capacity of high-BDP links, which takes long time.

Inaccurate congestion signal: Under the frequent handover ITSN scenario, packet losses may be due to handover or channel impairments. MPQUIC may misinterpret the unexpected loss signals as congestion and decrease cwnd afterward, degrading the network throughput.

Responsiveness: OLIA mainly relies on α in (1) to adapt to network conditions, and α is only updated when receiving an indication of packet loss. However, for unexpected

Algorithm 1: BDP Estimation in ITSN

Input : $\{P_t, d_r, N_r, \mathcal{C}^A_{r,t}, \mathcal{C}^N_{r,t}\}, \forall r \in \mathcal{R}$
Output: $\overline{\mathcal{B}_r}(t)$.
1 **Initialization at time** t_0
2 $t \leftarrow t_0$;
3 $\mathcal{C}^A_{r,t}, \mathcal{C}^N_{r,t} \leftarrow 0$;
4 $\mathcal{C}^A_{r,t} \leftarrow \eta \cdot W \log_2(1 + \frac{P_t g_1 g_2}{(4\pi d_r/\lambda)^2 N_r W})$;
5 Estimate $\mathcal{D}_{r,t}$ using Eq. (11);
6 **if** $t == t_0$ **then**
7 $\overline{\mathcal{B}_r}(t) \leftarrow \mathcal{C}^A_{r,t} * \mathcal{D}_{r,t}$;
8 **return** $\overline{\mathcal{B}_r}(t)$;
9 **else**
10 **while** *new ACK received at* t **do**
11 Update S_t, S_{t-1}, τ_r;
12 $\mathcal{C}^N_{r,t} \leftarrow \frac{S_t - S_{t-1}}{\Delta t}$;
13 Update $\mathcal{C}^N_{r,t}$ using AKF;
14 $\mathrm{C}_{r,t} = \min\{\mathcal{C}^A_{r,t}, \mathcal{C}^N_{r,t}\}$;
15 $\overline{\mathcal{B}_r}(t) = \frac{1}{\tau_r} \int_{t-\tau_r}^{t} \mathcal{C}_{r,t} * \mathcal{D}_{r,z} dz$;
16 **return** $\overline{\mathcal{B}_r}(t)$

events such as topology change, OLIA cannot perceive it, leading to a slow response in terms of cwnd adjustment. Assuming in the state s_2, the two disjoint paths both have an available bandwidth of 200 Mbps, the cwnd of F_0 and F_1 can be up to about 1000 MSS. After the state changes from s_2 to s_3 if F_0 hands over from G_1 to G_2, F_0 and F_1 have to share the bottleneck links where the bandwidth is 200 Mbps. In this case, if OLIA is unaware of the state change and keeps w_0 and w_1 at 1000 MSS unchanged, the overflow would occur at the bottleneck links.

The root cause of these problems boils down to one key challenge: MPQUIC at the transport layer is unable to differentiate between fluctuations in network conditions caused by congestion and those caused by mobility and handover. Thus, a mobility-aware congestion control algorithm for MPQUIC (MACO) is proposed, consisting of two components: BDP-Inspired Quick Start and Mobility-Aware Congestion Avoidance.

4 BDP-Inspired Quick Start

In this section, a quick start (QS) alternative is proposed to tackle the bandwidth under-utilization issue during the SS phase.

Since path BDP reflects the network capacity, it is wise to set the SS threshold (SST) at BDP first, as cwnd can quickly approach SST. Here, two key points should be considered: how to capture the variable BDP accurately at a low cost (**Algorithm 1**), and how to quickly approach the network capacity without severe congestion consequences (**Algorithm 2**).

4.1 BDP Estimation in ITSN

By definition, the BDP of path r at time t, $\mathcal{B}_r(t)$, is the product of the available bottleneck bandwidth of the tagged flow, $\mathcal{C}_{r,t}$, and the round-trip propagation delay $\mathcal{D}_{r,t}$. **Algorithm 1** summarizes the procedures of BDP calculation. Lines 1–8 aim to obtain the path BDP in the first RTT, and lines 9–15 present how to utilize the feedback received to further improve the BDP estimation accuracy. The details of these two parts are given in Sections 4.1.1 and 4.1.2, respectively.

4.1.1 Bottleneck at Access Links

As stated in [53], the bandwidth of ground-to-satellite wireless links is relatively low compared to other optical wired or wireless links, so the access link is likely the bottleneck. Under this assumption, we can derive the bottleneck bandwidth without lengthy network probing. In particular, the sender could quickly realize the access link status in the first RTT, as depicted in lines 6–8 of **Algorithm 1**, and initiate the data transmission over each path. This feature proves advantageous in scenarios where the RTT is excessively long.

To gain insights into the realistic situation of LEO access networks, we acquired several Starlink dishes and subscribed to LEO services provided by SpaceX so that we can measure the realistic E2E path condition changes over time. By conducting pings to a peered device in Seattle, US from Victoria, Canada, we have captured the fluctuations in network bandwidth, RTT, and packet drop rate over a subflow. The data traces from a 100-second interval on April 21, 2023, are depicted in Fig. 4. With the observation from extensive measurement studies, we have noted that the handover between the end host and satellites occurs approximately every 15 seconds. This frequent handover results in significant fluctuations in the throughput performance as shown in Fig. 4(a). However, due to the periodic satellite movements, the change of throughput appears good regularity so that predicting the bandwidth of access links without probing is feasible.

Denote by $\mathcal{C}^A_{r,t}$ the time-varying bandwidth associated with ground-satellite links. Recall the description of $\{v, d_1, d_2, R_1, R_2\}$ in Section 3.1, $\frac{d_1}{v} = \frac{2R_2 - R_1}{2v}$ defines the interval of state changes from the disjoint to shared state, e.g., from s_2 to s_3, and $\frac{d_2}{v} = \frac{2R_2 - 2d_1}{v}$ characterizes the interval of opposite changes, that is, from the shared to disjoint state. As a result, we can predict which satellite will be associated with subflow r at time t, as well as the distance between access satellites and H_1. Let $d_r(t)$ be the distance of F_r to their accessed satellites at time t, using the path-loss model, we have [54], [55]

$$\mathrm{SNR_r} = \frac{P_t g_1 g_2}{(4\pi d_r/\lambda)^2 N_r W}. \tag{2}$$

In (2), P_t stands for the transmit power, g_1 is the transmitting antenna gain, g_2 is the receiving antenna gain, λ is the signal wavelength, N_r is the noise power spectrum density (watts per hertz), and W denotes the bandwidth of the spot beam. Here we omit the symbol t of each parameter for simplicity.

Finally, the data rate of the ground-satellite link can be estimated by

$$\mathcal{C}^A_{r,t} = \eta \cdot W \log_2(1 + \mathrm{SNR_r}), \tag{3}$$

where $\eta \in (0, 1)$ is the efficiency coefficient of the system, depending on many factors, e.g., hardware and software design, as well as the modulation and coding schemes.

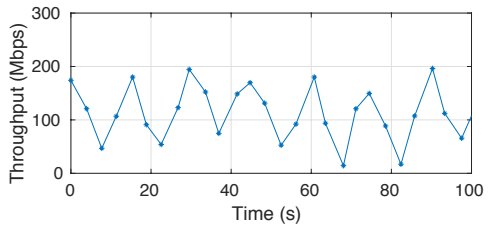

(a) Throughput changes over time

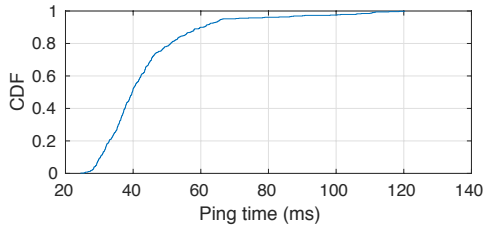

(b) The CDF of ping time with a subflow

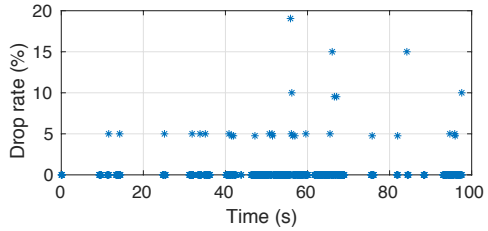

(c) The drop rate distributions over time

Fig. 4. Measurements over Starlink LEO networks.

4.1.2 Bottleneck at the Network Side

In the above subsection, we operated under the assumption of the existence of direct links between end hosts and satellites, where the link capacity typically mirrors the bottleneck bandwidth. In this subsection, we focus on how to determine the bottleneck link capacity in scenarios where direct links between end hosts and satellites are lacking, or when subflows encounter bottlenecks at non-access links, such as inter-satellite links or terrestrial networks, referred to as bottlenecks at the network side. Denote by $\mathcal{C}_{r,t}^N$ the time-varying bottleneck bandwidth at the network side.

Since bottlenecks could occur on any intermediate links that make up the connection, the sender can estimate $\mathcal{C}_{r,t}^N$ by measuring acknowledgments (ACKs). Lines 11–13 of **Algorithm 1** describe two steps to derive $\mathcal{C}_{r,t}^N$: real-time measurement based on ACK packets, and correction with the Adaptive Kalman Filter (AKF).

Given the self-clocking feature, a common approach to measure $\mathcal{C}_{r,t}^N$ is to send a few packets back-to-back over subflow r, and then monitor the timestamps of the received ACKs to estimate bottleneck bandwidth. Assuming S_t and S_{t-1} are the total amounts of data received by the mobile host at successive measurement time instants t and $t-1$, $\mathcal{C}_{r,t}^N$ is measured with

$$\mathcal{C}_{r,t}^N = \frac{S_t - S_{t-1}}{\Delta t}. \tag{4}$$

However, the measured $\mathcal{C}_{r,t}^N$ in this manner is likely biased due to many reasons, e.g., the sending window is too small during slow-start to match the actual network capacity so that the instantaneous $\mathcal{C}_{r,t}^N$ is much lower than it should be, or some neighboring satellites are unreachable due to angle issues so that the routing path is a detour, leading to a longer Δt and consequently an underestimated $\mathcal{C}_{r,t}^N$.

Therefore, we utilize an Adaptive Kalman Filter (AKF) [56] to remove the noise from the estimation of $\mathcal{C}_{r,t}^N$. Given limited measured samples, AKF can still quickly narrow down to the truth by taking a few of those inputs by understanding the variation or the uncertainty of those inputs. The standard Kalman filter goes through two stages to acquire the final estimate as follows.

The first stage is *prediction*, in which the estimated capacity ($\mathcal{C}_{r,t_e}^N$) of path r and the estimation errors $Z_{r,t}$ are updated as

$$\mathcal{C}_{r,t_e}^{N-} = \mathcal{C}_{r,t-1}^{N+} + \delta_{r,t}, \tag{5}$$
$$Z_{r,t}^{-} = Z_{r,t-1}^{+} + Q_r, \tag{6}$$

where the superscript "+" indicates that the estimate is a posterior, and "-" indicates a prior estimate. $\delta_{r,t}$ stands for white Gaussian noise with zero mean and variance Q_r, which depends on network uncertainties such as satellite mobility.

The second stage is *correction*. The measured network capacity is assumed disturbed by a white Gaussian noise $v_{r,t}$ with zero mean and variance R_r, such that

$$y_{r,t_m} = \mathcal{C}_{r,t_m}^N + v_{r,t}. \tag{7}$$

Here $\mathcal{C}_{r,t_m}^N$ is the instantaneously measured value at time t, using (4). Then the critical Kalman gain is derived by

$$K_{r,t} = Z_{r,t}^{-} \left(Z_{r,t}^{-} + R_r\right)^{-1}, \tag{8}$$

with which we can determine whether the predicted value or measured value is closer to the true value. Let $\hat{\mathcal{C}}_{r,t}^N$ and $\hat{Z}_{r,t}$ be the final correction for the predictions of $\mathcal{C}_{r,t_e}^{N-}$ and $Z_{p,t}^{-}$, we have

$$\hat{\mathcal{C}}_{r,t}^N = \mathcal{C}_{r,t_e}^{N-} + K_{r,t}\left(y_{r,t_m} - \mathcal{C}_{r,t_e}^{N-}\right), \tag{9}$$
$$\hat{Z}_{r,t} = Z_{r,t}^{-} - K_{r,t} Z_{r,t}^{-}. \tag{10}$$

The corrected values $\hat{\mathcal{C}}_{r,t}^N$ and $\hat{Z_{r,t}}$ will serve as the posterior states influencing future rounds of corrections. This approach results in a reduction of estimation errors over time, consequently reducing noise within $\mathcal{C}_{r,t}^N$[1].

4.1.3 $\mathcal{D}_{r,t}$ Estimation

$\mathcal{D}_{r,t}$ can be decomposed into the propagation delay $D_{\text{ul},t}$ and $D_{\text{dl},t}$ over the ground-to-satellite and satellite-to-ground links, and the delay $D_{\text{terr},t}$ within terrestrial networks. The former has significant variation due to the changing distance between ground stations and satellites. Since we can derive the distance d_r as described in the

1. To implement the Kalman filter effectively, knowledge of the covariances for prediction and measurement noise, denoted as Q_r and R_r, respectively, is essential. However, in our case, these parameters are initially unknown and may vary with changes in the network environment over time. To address this challenge, we can employ the Least Squares method to estimate them based on the autocorrelation of the innovation signal, as outlined in [57].

above subsection, $D_{\text{ul},t}$ and $D_{\text{dl},t}$ can be calculated by dividing the distance by the propagation speed, approximately 3×10^8 m/s. Comparatively, $D_{\text{terr},t}$ is more stable with fewer variations [58]. According to Fig. 4(b), the 99th percentile of the RTT for each subflow is 100 ms. Therefore, we can empirically set $D_{\text{terr},t}$ to a constant value at the first RTT. Upon receiving new ACKs in the subsequent rounds, the estimated delay could be updated, e.g., using an exponentially weighted moving average (EWMA).

Therefore, $\mathcal{D}_r$ is given by

$$\mathcal{D}_{r,t} = 2 * (D_{\text{ul},t} + D_{\text{dl},t} + D_{\text{terr},t}). \tag{11}$$

4.1.4 BDP Estimation

As summarized in **Algorithm 1**, after obtaining $\mathcal{C}^A_{r,t}$ and $\mathcal{C}^N_{r,t}$ through lines 4–13, $\mathcal{C}_{r,t}$ is given by

$$\mathcal{C}_{r,t} = \min\{\mathcal{C}^A_{r,t}, \mathcal{C}^N_{r,t}\}, \tag{12}$$

and the path BDP is derived by

$$\mathcal{B}_r(t) = \mathcal{C}_{r,t} * \mathcal{D}_{r,t}. \tag{13}$$

$\mathcal{B}_r(t)$ in (13) represents instantaneous BDP information immediately following the reception of a new acknowledgment. However, it does not consider the bandwidth fluctuations caused by the rapid movement of satellites during the subsequent transmission round. Therefore, directly utilizing $\mathcal{B}_r(t)$ to regulate cwnd settings is not ideal. To cope with this challenge, we average out the BDP within the successive RTT in the following manner,

$$\overline{\mathcal{B}_r}(t) = \frac{1}{\tau_r}\int_{t-\tau_r}^{t} \min\{\mathcal{C}^A_{r,z}, \mathcal{C}^N_{r,z}\} * \mathcal{D}_{r,z} dz, \tag{14}$$

in which $\overline{\mathcal{B}_r}(t)$ is used to guide the QS as presented in the next subsection.

4.2 QS

The key idea behind the QS is to set SST to the averaged BDP $\overline{\mathcal{B}_r}(t)$ in the first RTT. Next, to approach SST faster, we set the initial window of each subflow r, denoted by $\Omega_r(t)$ to a larger value based on historical information, rather than a small constant all the time. **Algorithm 2** states how the QS performs in a general case where the number of established subflows might be greater than 2.

For ease of understanding, we take a two-subflows example as shown in Fig. 5 to elaborate the QS design as follows.

When MACO users join the network and the first subflow F_0 is created, there is no historical information for the F_0. When the w_0 is below 4 maximum segment size (MSS), it is impossible to trigger fast retransmission to recover lost packets, and thus w_0 is initially set to 4 MSS, i.e., $\Omega_0(t_0) = 4$ MSS as shown in Fig. 5. Starting with $\Omega_0(t_0)$, w_0 is increased by 1 MSS per ACK until reaching the SST.

Because MPQUIC subflows share some similarities w.r.t. access link capacity, E2E hop count, packet loss rate, etc., the window change trajectory of F_0 is valuable in guiding the selection of $\Omega_1(t)$ for F_1. Suppose F_0 has sent a certain amount of data and experienced network congestion subsequently. We record the associated cwnd information ($w^*_0(t)$) whenever congestion occurs and store them into a set $\mathcal{W}_0$, i.e., $\mathcal{W}_0 = \{\{\, w^*_0(t)\,\}\}$, as described in the line 4 of **Algorithm 3**. Therefore, when starting up F_1 at t_3 as shown in Fig. 5, the BDP of F_1 denoted by $\overline{\mathcal{B}_1}(t_3)$ is first calculated using Eq. (14), and then F_1 checks if historical records exist. Since $\mathcal{W}_1$ is empty at t_3 while $\mathcal{W}_0$ has an element of $w^*_0(t_2)$, as depicted in lines 7–12 of **Algorithm 2**, $\Omega_1(t_3)$ would be determined by both $\overline{\mathcal{B}_1}(t_3)$ and $\mathcal{W}_0$ in the following way

$$\Omega_1(t_3) = \gamma \cdot \min\{\overline{\mathcal{B}_1}(t_3), w^*_0(t_2)\}. \tag{15}$$

Here we introduce a coefficient γ to ensure the initial window is not only large enough but also safe to start, and empirically, γ is set to $1/2$.

After states s_1 and s_2, both F_0 and F_1 have the transmission records and maintain their own set $\mathcal{W}_r$ ($r = \{0, 1\}$) for the subsequent states reference. Thereby, when F_r enters into the SS process again upon the occurrence of timeout or connection breakage, the corresponding $\Omega_r(t)$ can be generalized as

$$\Omega_r(t) = \gamma \cdot \min\{\overline{\mathcal{B}_r}(t), \max\{w^*_r(t)\}\}, \tag{16}$$

which corresponds to the lines 3–5 in **Algorithm 2**.

In conclusion, in the QS procedure, MACO strives to start with an appropriate Ω by learning from the recent past and taking advantage of good similarity among different subflows in the ITSN scenario; after the cwnd reaches the SST, MACO steps into CA phase as elaborated in the following subsections.

Algorithm 2: QS

Input : $\mathcal{W}_r, \forall r \in \mathcal{R}$
Output: cwnd value during the SS phase.

1 **if** *a new subflow F_r is created or a broken subflow is reconnected* **then**
2 // Set an initial cwnd for F_r
3 **if** $\mathcal{W}_r \neq \varnothing$ **then**
4 $w_{\max} \leftarrow \max\{w_r(t)\}$;
5 $\Omega_r(t) = \gamma \cdot \min\{\overline{\mathcal{B}_r}(t), w_{\max}\}$;
6 **else**
7 **if** $\exists \quad \mathcal{W}_q \quad \neq \varnothing$ **then** $q\in\mathcal{R}(q\neq r)$
8 $w_{\max} \leftarrow 0$;
9 **foreach** $q \in \mathcal{R}(q \neq r)$ **do**
10 **if** $w_{\max} < \max\{w_q(t)\}$ **then**
11 $w_{\max} \leftarrow \max\{w_q(t)\}$;
12 $\Omega_r(t) \leftarrow \gamma \cdot \min\{\overline{\mathcal{B}_r}(t), w_{\max}\}$;
13 **else**
14 $\Omega_r(t) \leftarrow 4$ MSS;
15 $w_r \leftarrow \Omega_r$;
16 **else**
17 // Increase the cwnd exponentially with RTT
18 $w_r \leftarrow w_r +$ # of ACKs ;
19 **return** w_r

Algorithm 3: Mobility-Aware Congestion Avoidance

Input : $\{w_r, \tau_r, \mathcal{C}_r(t-1), \mathcal{D}_r(t-1), TP_r(t)\}$, $\forall r \in \mathcal{R}$

Output: cwnd changes during the CA phase.

1 $Con\_1 \Leftarrow \mathbf{1}\{TP_r(t) < \mathcal{C}_r(t-1)\}$;
2 $Con\_2 \Leftarrow \mathbf{1}\{\tau_r(t) > \mathcal{D}_r(t-1) + \Delta_R\}$;
3 **if** *packet loss* $\wedge$ Con_1 $\wedge$ Con_2 **then**
4 $\mathcal{W}_r \leftarrow \mathcal{W}_r \cup w_r$;
5 $w_r \leftarrow w_r/2$;
6 **else**
7 $T_r = \max_{t \in \{t_0, t_1, \cdots, t_n\}} \tau_r(t)$;
8 **foreach** $k \in \mathcal{R}$ **do**
9 $x_k \leftarrow \frac{w_k(t_n)}{\tau_k(t_n)}$;
10 $w_r \leftarrow w_r + \frac{3 \max_{r \in \mathcal{R}} x_r^2 \sqrt{T_r}}{2\tau_r \left(\sum_{k \in \mathcal{R}} x_k\right)^{\frac{5}{2}}}$;
11 **return** w_r

5 Mobility-Aware MPQUIC Congestion Avoidance

Due to high-speed satellite movement, frequent handovers severely impair the quality of experience (QoE) for users [59]. To provide good QoE, the CA design is driven by three goals: 1) Distinguish the congestion loss from handover loss to avoid unnecessary cwnd reduction. 2) Maintain fast convergence to the network capacity. 3) The total throughput of multiple subflows in the handover process should be no less than the throughput that a single-path TCP can achieve. **Algorithm 3** concludes the CA design part.

5.1 Mobility-Aware Factor Design

For each subflow r, a mobility-aware factor $h_r \in \{0, 1\}$ is introduced to help identify the true congestion signal. According to lines 1–3 of **Algorithm 3**, MACO takes into account three conditions to detect if the network is congested, i.e., packet loss signal along with two conditions given in (17). Only if the three conditions are both satisfied, the network is identified as congested and $h_r = 1$. Otherwise, $h_r = 0$.

$$\begin{cases} TP_r(t) < \mathcal{C}_r(t-1), \\ \tau_r(t) > \mathcal{D}_r(t-1) + \Delta_R, \end{cases} \tag{17}$$

where $TP_r(t)$ is the available bandwidth measured by (4) at the t-th sampling time when receiving an ACK, while $\mathcal{C}_r(t-1)$ is the predicted access link bandwidth by (3) at the $(t-1)$-th sampling time right before sending packets. Similarly, $\tau_r(t)$ is the measured RTT at time t, and $\mathcal{D}_r(t-1)$ is the estimated propagation delay using (11) at time $t-1$. Considering the unavoidable estimation error of delay, Δ_R is a factor that represents the standard deviation of the differences between the recent RTT measurements and the corresponding estimated ones.

5.2 CA Design

In general, the CA algorithm devises a specific control policy governing the increase term (U_r) for each acknowledgment and the decrease term (V_r) triggered by packet loss signals.

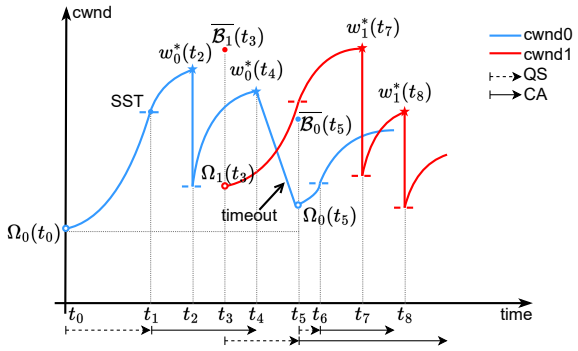

Fig. 5. Window growth model of MACO.

In our model, V_r is intrinsically tied to system stability and is typically set to half of the current congestion window, i.e., $V_r = \frac{w_r}{2}$. This value remains constant, and our primary focus centers on the design of U_r for each subflow r.

To meet the fast convergence goal, the AIMD scheme is undesirable in high-BDP networks. Instead, a function that grows aggressively when the current cwnd is far away from BDP and grows conservatively when the cwnd is approaching the BDP is more desirable. The square-root function presented in the recent proposal named Elastic-TCP [60] can fulfill our requirements with low complexity, so we employ a similar function to design U_r for each subflow r in the CA phase. Fig. 5 depicts how the cwnd is tuned with the square root increasing model during the CA phase.

Authors in [61], [62] formulated the CA process of MPTCP as a fluid model to facilitate the analysis of certain flow level properties, e.g., friendliness, convergence, and stability. [61] concluded that $\frac{\partial \phi_r(\mathbf{X}_\mathcal{R})}{\partial \mathbf{X}_\mathcal{R}}$ determines the convergence speed to the equilibrium locally if the system is perturbed by unexpected factors (e.g., handover), where ϕ_r is the ratio of U_r to V_r and $\mathbf{X}_\mathcal{R}(t) = (x_r(t), r \in \mathcal{R})$, and $x_r = w_r/\tau_r$, indicating the transmission rate on subflow r.

Let $x_r(t) = w_r(t)/\tau_r$ denote the transmission rate of subflow r at time t

To achieve the same convergence property as Elastic-TCP, MACO should have

$$\left(\frac{\partial \phi_r}{\partial \mathbf{X}_\mathcal{R}}\right)^{MACO} = \left(\frac{\partial \phi_r}{\partial \mathbf{X}_\mathcal{R}}\right)^{Elastic-TCP}. \tag{18}$$

In addition, according to the Theorems in [62], an equilibrium of the system does exist if $\phi_r(\mathbf{X}_\mathcal{R})$ of MACO can be generalized as

$$\phi_r(\mathbf{X}_\mathcal{R}) = \frac{\theta_r}{x_r}, \tag{19}$$

where $\theta_r > 0$ is a variable depending on different convergence rate requirements.

Since

$$\left(\frac{\partial \phi_r}{\partial \mathbf{X}_\mathcal{R}}\right)^{Elastic-TCP} = -\frac{3\sqrt{T_r x_r^{TCP}}}{\tau_r^2 (x_r^{TCP})^3}, \tag{20}$$

where T_r is the maximum RTT the subflow r has ever experienced, which will be updated upon reception of a new ACK, we have

$$-\frac{\theta_r}{x_r^2} = -\frac{3\sqrt{T_r}}{\tau_r^2 (x_r^{TCP})^{\frac{5}{2}}}. \tag{21}$$

In addition, to ensure goal 3) that the multiple subflows maintain at least the same aggregate throughput as co-existing Elastic-TCP, we have $\sum_{k\in\mathcal{R}} x_k = \max_{r\in\mathcal{R}} \left(x_r^{TCP}\right)$. Furthermore,

$$\max_{r\in\mathcal{R}} \left(x_r^{TCP}\right)^{\frac{5}{2}} = \left(\sum_{k\in\mathcal{R}} x_k\right)^{\frac{5}{2}} = \max_{r\in\mathcal{R}} \frac{3x_r^2\sqrt{T_r}}{\theta_r \tau_r^2}. \tag{22}$$

Then,

$$\theta_r = \frac{3\max_{r\in\mathcal{R}} x_r^2\sqrt{T_r}}{\tau_r^2 \left(\sum_{k\in\mathcal{R}} x_k\right)^{\frac{5}{2}}}. \tag{23}$$

Hence, we obtain

$$\phi_r\left(\mathbf{X}_{\mathcal{R}}\right) = \frac{3\max_{r\in\mathcal{R}} x_r^2\sqrt{T_r}}{\tau_r^2 x_r \left(\sum_{k\in\mathcal{R}} x_k\right)^{\frac{5}{2}}}. \tag{24}$$

Given V_r, we can obtain the solution of the increment term $U_r\left(\mathbf{X}_{\mathcal{R}}\right)$ as below,

$$U_r\left(\mathbf{X}_{\mathcal{R}}\right) = \frac{3\max_{r\in\mathcal{R}} x_r^2\sqrt{T_r}}{2\tau_r \left(\sum_{k\in\mathcal{R}} x_k\right)^{\frac{5}{2}}}. \tag{25}$$

Finally, The CA algorithm is summarized in **Algorithm 3**:

- In the CA phase, for each ACK on F_r,

$$w_r \leftarrow w_r + \frac{3\max_{r\in\mathcal{R}} x_r^2\sqrt{T_r}}{2\tau_r \left(\sum_{k\in\mathcal{R}} x_k\right)^{\frac{5}{2}}}, \tag{26}$$

5.3 Time complexity analysis

In this subsection, we briefly analyze the complexity of our algorithms in terms of time consumption.

In **Algorithm** 1, the operations of each step can be done in constant time, so the time complexity is $O(1)$.

For **Algorithm** 2, the time complexity is mainly affected by line 4 and lines 9–12. To find out the maximum $w_r(t)$ in the set $\mathcal{W}_r$ in line 4, we may need to compare each element with the current maximum in the worst case. Therefore, line 4 has a time complexity of $O(m)$ where m stands for the number of occurrences of congestion over path r. The task of lines 9–12 is to search the maximum value across $R-1$ sets, where R indicates the number of subflows that MPQUIC has established and used. Under the assumption that each subflow maintains the same magnitude of the number of congestion occurrences, the running time of lines 9–12 is $mR-m$. As a result, the time complexity of **Algorithm** 2 is $O(mR)$.

Similarly, in **Algorithm** 3, the line 7 and lines 8–9 contribute n and R running times, respectively. Here n represents the number of RTT records for a certain path. Consequently, the overall time complexity is $O(n+R)$.

6 Performance Evaluation

In this section, we conduct extensive experiments to verify the performance of MACO in the ITSN scenario, in comparison with the following benchmarks:

1) BBR: Similarly to ours, BBR is a BDP-inspired congestion control algorithm, which has been extensively studied in satellite networks thanks to its BDP-aware features. BBR with multipath support is not yet available since the coupled design of the pacing gain rate for multiple paths remains an open issue. Therefore, we currently use BBR as the single-path benchmark in ITSN scenarios.
2) OLIA: OLIA has been widely adopted as the congestion control algorithm for MPQUIC. It aims to achieve the Pareto-optimal cwnd regulation and good fairness towards single-path users. Extensive experiments demonstrate that OLIA achieves great bandwidth utilization under various network settings.

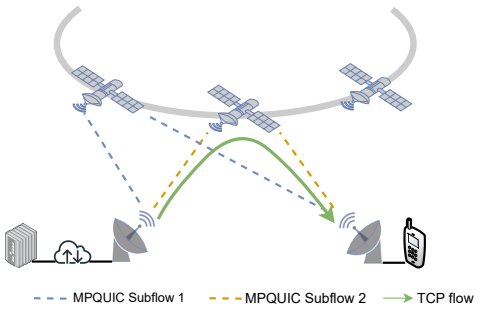

Fig. 6. Simulation topology.

In comparison with single-path-based (i.e., BBR) and multipath-based (i.e., OLIA and MACO) solutions in mobile environments, we can gain insights into the efficiency of multipath transmission in dealing with seamless handover. With respect to the multipath packet scheduling policy, we employ the round-robin algorithm for all multipath-based solutions. On the other hand, the comparison between loss-based (i.e., OLIA) and BDP-based (i.e., BBR and MACO) solutions reveals how they react to high BDP networks and how the E2E QoS performance will be affected.

6.1 Prototype Implementation

To begin with, we extended the existing QUIC module [63] to MPQUIC based on ns-3 in accordance with the Internet Engineering Task Force (IETF) draft[2] on MPQUIC. We refer readers to [20] and our open-source code at https://github.com/ssjShirley/mpquic for the implementation details of MPQUIC-ns3.

Based on the MPQUIC prototype, we further create two mobility modules: one for the LEO satellite constellation, and the other for facilitating end devices interacting with the LEO satellites. They are responsible for configuring and maintaining the position of satellites and end hosts. As satellites move, end hosts can continuously calculate their distance to orbiting satellites, while also assessing the SNR of each interface.

To let the transport layer be aware of the SNR changes at the link layer, as illustrated in Fig. 7, we introduce a database in the control plane to enable the cross-layer interactions on which the MACO algorithm is implemented.

2. https://datatracker.ietf.org/doc/draft-deconinck-quic-multipath/

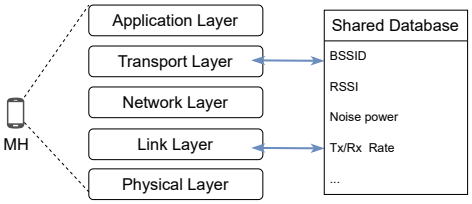

Fig. 7. Cross-layer architectural blueprint.

TABLE 3
The setting for parameters in (2) and (3)

Parameters	Value
g_1	37.7 dBi
g_2	37.1 dBi
λ	0.086 m
N_r	1.6×10^{-20} W/Hz
η	0.98
W	12.5 MHz

Through the creation of interfaces that connect the layers to the database, the data stored in the database is accessible to protocol functions across different layers. For instance, whenever the access link conditions change, the link layer acquires parameters such as Basic Service Set Identifier (BSSID), Received Signal Strength Indicator (RSSI), etc. These parameters are then recorded in the database, enabling the transport layer to retrieve this information. Note that the presence of the database does not change the conventional layered structure, and the encapsulation and decapsulation processes do not involve the data stored in the database. Therefore, this architecture is backward compatible.

6.2 Experimental Scenario and Settings

Fig. 6 depicts the topology we used, in which a client and a server engage in communication through two satellites. Two MPQUIC subflows are established between the sender and the receiver. Concurrently, background TCP flows are generated to traverse through the same satellites, competing with the MPQUIC flows.

According to the parameters outlined in [64] and the specifications reported by Starlink[3], we simulated an LEO satellite constellation with an altitude of 550 km, and the distance between two adjacent satellites in the same orbit R_1 is set to 150 Km. The satellite's moving speed is 7 km/s, and each satellite has a footprint diameter of about 460 km.

By referring to recent studies [54], [65], [66], some parameter settings in (2) and (3) are given in Table 3. Combining with our measurement results presented in Fig. 4(a), which shows the achieved throughput, we configure the transmit power P_t. For instance, considering that the throughput peaks at 200 Mbps when the distance is minimized to 550 km, we assign values of 200 Mbps and 550 km to $\mathcal{C}_{r,t}^{A}$ in (3) and d_r in (2), respectively. By substituting these values into (3) and (2), P_t is 35.12 dBm.

3. https://www.astronomy.com/space-exploration/starlink-satellite-streaks-how-big-of-a-problem-are-they/

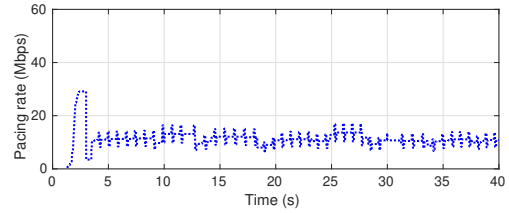

(a) The pacing rate adaptation of BBR

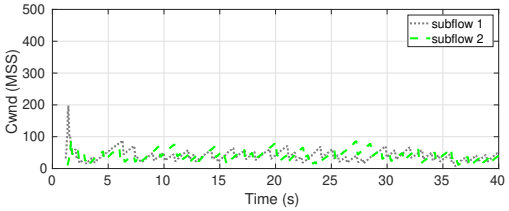

(b) cwnd of OLIA

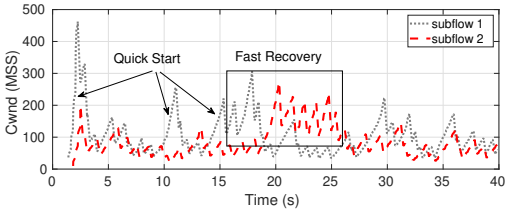

(c) cwnd of MACO

Fig. 8. The cwnd adaptation of different algorithms over time.

6.3 Experimental Results

With the settings above, we compare MACO with benchmark algorithms in terms of four aspects: cwnd adaptation, throughput, TCP friendliness, convergence, and the impact of satellite density and BDP.

6.3.1 Congestion Window Adaptation

The cwnd is a critical aspect of congestion control design, as it illustrates how an algorithm adjusts its cwnd in response to changing network dynamics. For BBR which does not employ a traditional cwnd concept, we rely on the pacing rate as an indicator of its adaptive behavior. Fig. 8 presents the cwnd regulation over time.

With an average RTT of 100 ms, it's noteworthy that 500 MSS is roughly equal to an effective sending rate of 60 Mbps. An insightful observation can be drawn from the data depicted in Fig. 8, that is, MACO consistently maintains the largest cwnd on average, followed by BBR, with OLIA displaying the smallest cwnd.

Fig. 8(a) illustrates the frequent oscillation in the pacing rate of the BBR congestion control algorithm. This behavior arises from BBR's aim to keep router queues at the bottleneck link consistently empty by precisely matching the bottleneck link's rate limit. When a BBR flow coexists with another NewReno flow over a shared bottleneck, the latter tends to aggressively fill up the queue until packet loss occurs. In contrast, BBR triggers its draining function to empty the queue, which, in turn, limits its pacing rate. Consequently, the pacing rate of BBR is suppressed when it shares the bottleneck link with other traffic.

Comparing the cwnd trace of OLIA with MACO as shown in Fig. 8(b) and Fig. 8(c), respectively, it is evident that MACO maintains a higher average cwnd. This outcome can be attributed to MACO's QS and fast recovery mechanisms. In scenarios involving both mobility and competing traffic, the likelihood of packet losses increases. Unlike MACO, OLIA cannot distinguish congestion-induced losses from losses caused by mobility. As a result, cwnd degradation occurs frequently in OLIA, limiting the cwnd to under 100 MSS after 5 seconds. This value is significantly smaller than MACO's counterpart, which is 300 MSS.

6.3.2 Throughput

Fig. 9 demonstrates the throughput of each algorithm under the impact of TCP background traffic. By comparing the throughput of BBR, OLIA, and MACO, we observe that they all suffer from frequent fluctuations in the presence of satellite movement. On the other hand, the throughput of BBR ranges from 5 Mbps to 15 Mbps, which is comparatively low because BBR is a single-path-based solution. Nevertheless, BBR outperforms OLIA after 22 seconds even though OLIA reaches 38 Mbps in the first 22 seconds. This result reveals that the loss-based congestion control is not suitable for the high-BDP as well as highly lossy networks. Compared to BBR and OLIA, the throughput curve of MACO fits the Starlink measurements shown in Fig. 4(a) better, and that is the reason why MACO can achieve up to three times higher throughput record.

Fig. 10 illustrates the CDF of per-packet E2E delay with different algorithms. The 95th percentile of E2E delay is 101 ms for MACO, and the counterparts of OLIA and BBR are 130 ms and 132 ms, respectively. It implies that the throughput improvement achieved by MACO does not lead to longer queuing delays.

As analyzed earlier, filtering out non-congestion-related loss signals from congestion-related loss signals is crucial for throughput improvement as the large proportion of non-congestion-related loss leads to unnecessary cwnd decrement. We measured the number of congestion losses detected by different algorithms. In this scenario, MACO and BBR both receive a similar number of congestion signals, specifically 71 and 69 respectively. However, OLIA experiences a much higher number of congestion losses, totaling 128, leading to significant degradation of its cwnd.

6.3.3 TCP Friendliness

TCP-friendliness is a crucial characteristic of multipath congestion control algorithms. It ensures that the combined throughput of multiple subflows sharing a bottleneck with TCP flows does not exceed the throughput achieved by TCP. When the bandwidth is limited while both TCP and MPQUIC request a large amount of bandwidth, we need to consider it to ensure fairness. However, if the bandwidth resources are sufficient or the TCP user does not request much bandwidth, MPQUIC can still grab more bandwidth as demand. In our experiments, handover occurs every 15 seconds, resulting in the two MPQUIC subflows accessing the same satellite and sharing the bottleneck with TCP background traffic regulated by NewReno every 30 seconds, as shown in Fig. 3. The bottleneck-shared events are marked in Fig. 9(b) and 9(c). The aggregated throughput of OLIA or MACO is nearly equal to or lower than that of TCP during these events, indicating their TCP friendliness. Furthermore, MACO demonstrates TCP friendliness while also striving for higher throughput. It achieves this by aggressively increasing the congestion window when the network capacity is far from being reached and adopting a more conservative approach as it approaches the network capacity. Although OLIA meets the requirement of TCP friendliness, it fails to outperform TCP whenever there is no shared bottleneck.

6.3.4 Convergence

Since the system could be affected by unexpected factors in ITSN, e.g., satellite availability and weather conditions, maintaining a fast convergence to the network capacity is crucial. To evaluate the convergence performance, we measure the recovery time from the moment that the subflow enters a specific phase (i.e., SS or CA) until the moment that the cwnd reaches the path BDP.

In the existence of TCP flows, we observe that MACO is more responsive during either stage compared to OLIA, which is the major reason behind the throughput and delay improvement as depicted in Fig. 9 and Fig. 10. Fig. 11(a) shows that the 99th percentile of the recovery time in the SS phase for MACO and OLIA is 129.4 ms and 470.3 ms, respectively, and the counterpart in the CA phase for MACO and OLIA is 204 ms and 770.3 ms, respectively. On the other hand, compared to the convergence performance in the case without competing traffic, the recovery time of MACO and OLIA in the CA stage is increased by 22.7% and 30.8%, respectively. The comparison results demonstrate that MACO substantially optimizes the system convergence against OLIA in various scenarios.

6.3.5 The Impact of Satellite Density and BDP

Over time, an increasing number of satellites are being launched, resulting in denser satellite distributions across space. In this subsection, we conduct a series of experiments investigating how the satellite density affects the performance of each algorithm. Here we systematically tune the value of inter-satellite distance R_1 to adjust the satellite density. The smaller the R_1, the denser satellites are deployed. For various applications, including file transmission, the time it takes to complete the transfer of a specific file size serves as a critical performance metric that gauges the effectiveness of a congestion control algorithm. Therefore, the completion time is adopted as a metric for performance evaluation.

In addition, we aim to discover the influence of the changing BDP on the completion time of file transmission. Given the BDP is dependent on both bandwidth and delay, we manipulate the two parameters individually to discover how each of them affects the results. Unless specified otherwise, all other configurations, such as transmit power and satellite moving speed, remain consistent with the settings mentioned above.

Fig. 12 depicts our findings on how link bandwidth influences the completion time when transmitting a 10 MB file at various R_1 values. From these results, two key observations can be made. Firstly, increasing bandwidth is beneficial for MACO to speed up the file transfer algorithm. However, for BBR and OLIA, incremental bandwidth fails

This article has been accepted for publication in IEEE Transactions on Mobile Computing. This is the author's version which has not been fully edited and content may change prior to final publication. Citation information: DOI 10.1109/TMC.2024.3397164

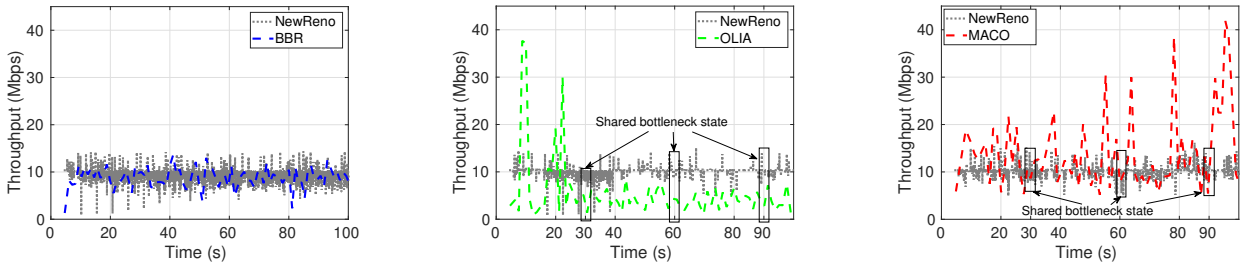

Fig. 9. Throughput performance of each algorithm when processing QUIC traffic in the presence of TCP background traffic controlled by NewReno: (a) BBR, (b) OLIA, (c) MACO.

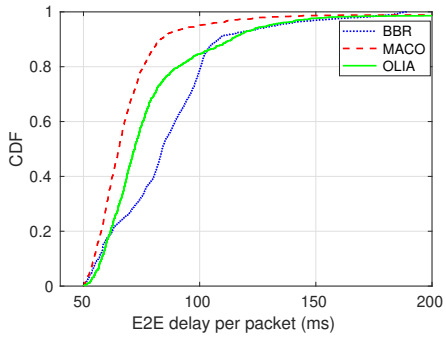

Fig. 10. The CDF of E2E packet delay.

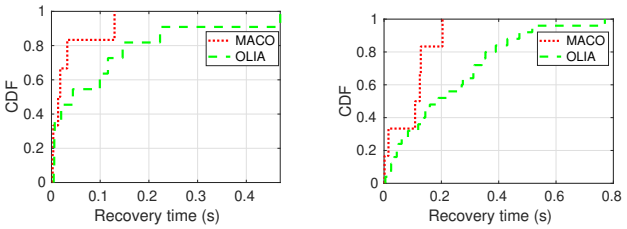

Fig. 11. Convergence analysis when background traffic exists.

to substantially decrease completion time when R_1 is either too long or too short. This is attributed to the challenges that BBR and OLIA face in fully utilizing bandwidth within highly lossy and mobile network environments. Secondly, higher satellite density proves advantageous in certain scenarios, as denser satellite distributions offer more stable access links and greater available link bandwidth. However, this advantage is not universally applicable, especially in cases where satellites are ultra-dense distributed and the handover happens frequently.

Specifically, when R_1 is less than or equal to 100 Km, we observe a reduction in completion time for all algorithms as bandwidth increases. OLIA decreases BBR's completion time by 7.3% to 38.22%, while MACO reduces OLIA by 8.5% to 64.2%. However, for scenarios where R_1 is 80 Km, completion times for BBR and OLIA initially decrease as bandwidth expands up to 20 MHz, but start to increase as bandwidth exceeds 20 MHz. BBR outperforms OLIA such that it has a 1.3% – 56.5% completion time reduction in this case, while MACO reduces the completion time of BBR and OLIA by up to 6.5 and 20.6 s, respectively. Therefore, MACO consistently achieves the shortest completion times across all scenarios. This relies on the advantages of MACO's ability to adapt to changes in bandwidth and employ multipath transmission in mobile settings.

Fig. 13 investigates how algorithms respond to changing delays in diverse mobile scenarios. In all scenarios, an increase in E2E propagation delay leads to prolonged completion times. MACO and OLIA outperform BBR when the delay is less than 250 ms as shown in Figures where $R_1 = 120$ and 100 Km. However, in scenarios where the delay surpasses this threshold, OLIA experiences performance degradation, resulting in significantly longer completion times compared to MACO and BBR. Conversely, MACO consistently achieves the shortest completion times across all scenarios. This can be attributed to its ability to consider measured path bandwidth and RTT, allowing it to distinguish congestion-related losses from handover losses. This approach mitigates unnecessary cwnd decreases and detrimental retransmissions, particularly in scenarios characterized by high delays.

In summary, the rising satellite density presents a dual-edged impact. While it can enhance link quality, it can also introduce more frequent handovers and a higher drop rate. When compared to BBR and OLIA, MACO consistently benefits from the increasing density. This is primarily due to MACO's ability to proactively reduce its cwnd to mitigate the risk of significant packet loss before handovers take place, and its rapid adaptation to network BDP changes in the presence of network perturbations. Additionally, MACO demonstrates better stability in response to fluctuations in bandwidth and delays.

7 Conclusion and Future Research Direction

This paper presents an analytical framework for MPQUIC-enabled ITSN and proposes a multipath congestion control algorithm called MACO, addressing three key challenges. First, MACO tackles the low efficiency of benchmark algorithms in ITSN by leveraging the regularity of LEO topology and predictability of satellite movements to realize network capacity within the first RTT without prohibitive network probing. Second, given the estimated network capacity and the similarity among subflows, MACO develops a quick

This article has been accepted for publication in IEEE Transactions on Mobile Computing. This is the author's version which has not been fully edited and content may change prior to final publication. Citation information: DOI 10.1109/TMC.2024.3397164

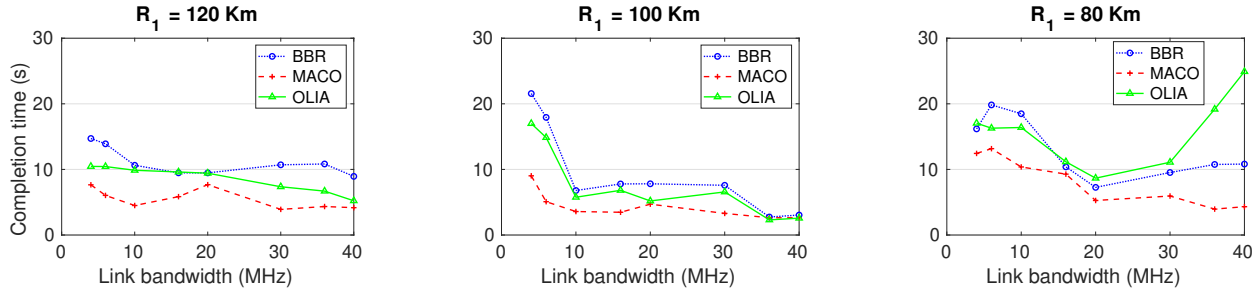

Fig. 12. The impact of link bandwidth on the completion time at varying satellite density.

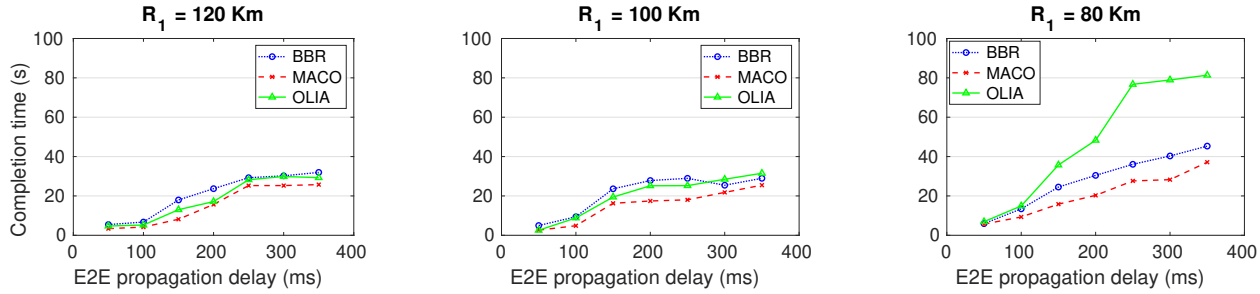

Fig. 13. The impact of propagation delay on the completion time at varying satellite density.

start (QS) mechanism to reduce the duration of the slow start (SS) phase. Lastly, MACO addresses the issue of unsatisfactory convergence by introducing a multipath-based fluid model to regulate cwnd on multiple subflows. Simulation results show that MACO reduces the completion time by 64.2% and achieves three times higher throughput against benchmark algorithms.

In this work, we study the case that all paths connect to the LEO satellite network. In future research, we will investigate new challenges to designing the congestion control algorithm for MPQUIC when the access network is heterogeneous, e.g., MPQUIC accesses to WiFi, 5G, unmanned aerial vehicle (UAV), and satellites simultaneously.

In the following research, we will consider the extension to moving end hosts. The moving patterns of terrestrial-based devices including end hosts and end-hosts can be summarized as two types: moving slow but hard to predict and moving fast but predictable. Since the moving speed of the first type of device is far slower than satellite movements, we can neglect such movements. For the case where the mobile user, e.g., a high-speed train, has lower but not negligible moving speed compared to satellites, future research can be done to predict the user mobility to correct the SNR estimation. The current congestion control design can still be applicable in this case.

REFERENCES

[1] D. Zhou, M. Sheng, J. Li, and Z. Han, "Aerospace integrated networks innovation for empowering 6G: A survey and future challenges," *IEEE Communications Surveys & Tutorials*, 2023.

[2] Y. Liu, L. Jiang, Q. Qi, K. Xie, and S. Xie, "Online computation offloading for collaborative space/aerial-aided edge computing toward 6G system," *IEEE Transactions on Vehicular Technology*, vol. 73, no. 2, pp. 2495–2505, 2024.

[3] N. Cheng, H. Jingchao, Y. Zhisheng, Z. Conghao *et al.*, "6G service-oriented space-air-ground integrated network: A survey," *Chinese Journal of Aeronautics*, vol. 35, no. 9, pp. 1–18, 2022.

[4] Z. Jia, M. Sheng, J. Li, and Z. Han, "Toward data collection and transmission in 6G space–air–ground integrated networks: Cooperative HAP and LEO satellite schemes," *IEEE Internet of Things Journal*, vol. 9, no. 13, pp. 10 516–10 528, 2021.

[5] W. Dai, H. Li, Q. Wu, and X. Wang, "NDM: Network driving IP mobility support in large scale LEO satellite network," in *IEEE Symposium on Computers and Communications (ISCC)*, 2020, pp. 1–7.

[6] J. Pan, R. Jain, S. Paul, and C. So-In, "MILSA: A new evolutionary architecture for scalability, mobility, and multihoming in the future Internet," *IEEE Journal on Selected Areas in Communications*, vol. 28, no. 8, pp. 1344–1362, 2010.

[7] V. Ishakian, J. Akinwumi, F. Esposito, and I. Matta, "On supporting mobility and multihoming in recursive Internet architectures," *Computer Communications*, vol. 35, no. 13, pp. 1561–1573, 2012.

[8] A. Ford, C. Raiciu, M. Handley, and O. Bonaventure, "RFC 6824: TCP extensions for multipath operation with multiple addresses," *Internet Engineering Task Force*, 2013.

[9] Q. De Coninck and O. Bonaventure, "Multipath QUIC: Design and evaluation," in *Proceedings of the 13th International Conference on Emerging Networking Experiments and Technologies*, 2017, pp. 160–166.

[10] W. Yang, S. Shu, L. Cai, and J. Pan, "MM-QUIC: Mobility-aware multipath QUIC for satellite networks," in *2021 17th International Conference on Mobility, Sensing and Networking (MSN)*. IEEE, 2021, pp. 608–615.

[11] X. Liu, T. Ma, Z. Tang, X. Qin, H. Zhou, and X. S. Shen, "UltraStar: A lightweight simulator of ultra-dense LEO satellite constellation networking for 6G," *IEEE/CAA Journal of Automatica Sinica*, vol. 10, no. 3, pp. 632–645, 2023.

[12] R. Khalili, N. Gast, M. Popovic, and J.-Y. Le Boudec, "MPTCP is not Pareto-optimal: Performance issues and a possible solution," *IEEE/ACM Transactions on Networking*, vol. 21, no. 5, pp. 1651–1665, 2013.

[13] R. Lübben and J. Morgenroth, "An odd couple: Loss-based congestion control and minimum RTT scheduling in MPTCP," in *IEEE 44th Conference on Local Computer Networks (LCN)*. IEEE, 2019, pp. 300–307.

[14] W. Wei, K. Xue, J. Han, D. S. Wei, and P. Hong, "Shared bottleneck-based congestion control and packet scheduling for multipath TCP," *IEEE/ACM Transactions on Networking*, vol. 28, no. 2, pp. 653–666, 2020.

[15] Y. Cao, M. Xu, and X. Fu, "Delay-based congestion control for multipath TCP," in *20th IEEE International Conference on Network Protocols (ICNP)*. IEEE, 2012, pp. 1–10.

[16] V. Arun and H. Balakrishnan, "Copa: Practical delay-based congestion control for the Internet," in *15th USENIX Symposium on Networked Systems Design and Implementation (NSDI 18)*, 2018, pp. 329–342.

[17] N. Cardwell, Y. Cheng, C. S. Gunn, S. H. Yeganeh, and V. Jacobson, "BBR: Congestion-based congestion control," *Communications of the ACM*, vol. 60, no. 2, pp. 58–66, 2017.

[18] M. Dong, T. Meng, D. Zarchy, E. Arslan, Y. Gilad, B. Godfrey, and M. Schapira, "{PCC} vivace:{Online-Learning} congestion control," in *15th USENIX Symposium on Networked Systems Design and Implementation (NSDI 18)*, 2018, pp. 343–356.

[19] N. Jay, N. Rotman, B. Godfrey, M. Schapira, and A. Tamar, "A deep reinforcement learning perspective on Internet congestion control," in *International Conference on Machine Learning*. PMLR, 2019, pp. 3050–3059.

[20] S. Shu, W. Yang, J. Pan, and L. Cai, "A multipath extension to the QUIC module for ns-3," in *Proceedings of the 2023 Workshop on ns-3*, 2023, pp. 86–93.

[21] N. Cardwell, Y. Cheng, C. S. Gunn, S. H. Yeganeh, and V. Jacobson, "BBR: Congestion-based congestion control: Measuring bottleneck bandwidth and round-trip propagation time," *Queue*, vol. 14, no. 5, pp. 20–53, 2016.

[22] D. Raychaudhuri, K. Nagaraja, and A. Venkataramani, "MobilityFirst: a robust and trustworthy mobility-centric architecture for the future Internet," *ACM SIGMOBILE Mobile Computing and Communications Review*, vol. 16, no. 3, pp. 2–13, 2012.

[23] L. Zhang, A. Afanasyev, J. Burke, V. Jacobson *et al.*, "Named data networking," *ACM SIGCOMM Computer Communication Review*, vol. 44, no. 3, pp. 66–73, 2014.

[24] J. Day, I. Matta, and K. Mattar, "Networking is IPC: a guiding principle to a better Internet," in *Proceedings of the 2008 ACM CoNEXT Conference*, Madrid, Spain, 2008, pp. 1–6.

[25] V. Jacobson, D. K. Smetters, J. D. Thornton, M. F. Plass *et al.*, "Networking named content," in *Proceedings of CoNEXT'09*. ACM, 2009, pp. 1–12.

[26] T. Koponen, M. Chawla, B.-G. Chun, A. Ermolinskiy, K. H. Kim, S. Shenker, and I. Stoica, "A data-oriented (and beyond) network architecture," in *Proceedings of the ACM SIGCOMM 2007 Conference*, 2007, pp. 181–192.

[27] D. Farinacci, V. Fuller, D. Meyer, and D. Lewis, "Locator/ID separation protocol (LISP)," *IETF Network Working Group RFC 6830*, 2013.

[28] R. Li, "New IP: Going beyond the limits of the Internet," in *a Keynote Speech at IEEE Globecom 2019, Hawaii*, 2019.

[29] J. McCauley, Y. Harchol, A. Panda, B. Raghavan, and S. Shenker, "Enabling a permanent revolution in Internet architecture," in *Proceedings of the ACM Special Interest Group on Data Communication*, 2019, pp. 1–14.

[30] Z. Zhang, B. Zhao, Z. Feng, W. Yu, and C. Wu, "MSN: A mobility-enhanced satellite network architecture: Poster," in *Proceedings of the 22nd Annual International Conference on Mobile Computing and Networking*, 2016, pp. 465–466.

[31] H. Xu, D. Li, M. Liu, G. Han, W. Huang, and C. Xu, "QoE-driven intelligent handover for user-centric mobile satellite networks," *IEEE Transactions on Vehicular Technology*, vol. 69, no. 9, pp. 10 127–10 139, 2020.

[32] Y. Xing, K. Xue, Y. Zhang, J. Han, J. Li, and D. S. Wei, "An online learning assisted packet scheduler for MPTCP in mobile networks," *IEEE/ACM Transactions on Networking*, vol. 31, no. 5, pp. 2297–2312, 2023.

[33] T.-T. Chu, M. A. Labiod, B. Augustin, and A. Mellouk, "GADaM on the road - Smart approach to multi-access networks: Analytical and practical evaluation in various urban mobile environments," in *2023 IEEE Wireless Communications and Networking Conference (WCNC)*. IEEE, 2023, pp. 1–6.

[34] Y. Xing, K. Xue, Y. Zhang, J. Han *et al.*, "A stream-aware MPQUIC scheduler for HTTP traffic in mobile networks," *IEEE Transactions on Wireless Communications*, vol. 22, no. 4, pp. 2775–2788, 2023.

[35] H. Shi, L. Zhang, X. Zuo, Q. Wu, H. Li, and Y. Cui, "Multipath deadline-aware transport proxy for space network," *IEEE Internet Computing*, vol. 25, no. 6, pp. 51–57, 2021.

[36] N. Dukkipati, T. Refice, Y. Cheng, J. Chu *et al.*, "An argument for increasing TCP's initial congestion window," *ACM SIGCOMM Computer Communication Review*, vol. 40, no. 3, pp. 26–33, 2010.

[37] Y. Li, R. Miao, H. H. Liu, Y. Zhuang *et al.*, "HPCC: High precision congestion control," in *Proceedings of the ACM Special Interest Group on Data Communication*, 2019, pp. 44–58.

[38] Y. Zhu, H. Eran, D. Firestone, C. Guo *et al.*, "Congestion control for large-scale RDMA deployments," *ACM SIGCOMM Computer Communication Review*, vol. 45, no. 4, pp. 523–536, 2015.

[39] R. Mittal, V. T. Lam, N. Dukkipati, E. Blem *et al.*, "TIMELY: RTT-based congestion control for the datacenter," *ACM SIGCOMM Computer Communication Review*, vol. 45, no. 4, pp. 537–550, 2015.

[40] I. Cho, K. Jang, and D. Han, "Credit-scheduled delay-bounded congestion control for datacenters," in *Proceedings of the ACM SIGCOMM'17*, New York, NY, USA, 2017, pp. 239–252.

[41] C. Raiciu and G. Antichi, "NDP: Rethinking datacenter networks and stacks two years after," *ACM SIGCOMM Computer Communication Review*, vol. 49, no. 5, pp. 112–114, 2019.

[42] B. Montazeri, Y. Li, M. Alizadeh, and J. Ousterhout, "Homa: A receiver-driven low-latency transport protocol using network priorities," in *Proceedings of the ACM SIGCOMM'18*, 2018, pp. 221–235.

[43] J. Wang, J. Liao, and X. Zhu, "Latent handover: A flow-oriented progressive handover mechanism," *Computer Communications*, vol. 31, no. 10, pp. 2319–2340, 2008.

[44] E. Kohler, M. Handley, and S. Floyd, "Designing DCCP: Congestion control without reliability," *ACM SIGCOMM Computer Communication Review*, vol. 36, no. 4, pp. 27–38, 2006.

[45] J. R. Iyengar, P. D. Amer, and R. Stewart, "Concurrent multipath transfer using SCTP multihoming over independent end-to-end paths," *IEEE/ACM Transactions on Networking*, vol. 14, no. 5, pp. 951–964, 2006.

[46] C. Xie, H. Hu, and Y. Liu, "Shared bottleneck detection for multipath transmission in high latency satellite network," in *2019 IEEE 7th International Conference on Computer Science and Network Technology (ICCSNT)*. IEEE, 2019, pp. 38–42.

[47] V. Jacobson, "Congestion avoidance and control," *ACM SIGCOMM computer communication review*, vol. 18, no. 4, pp. 314–329, 1988.

[48] L. Cai, X. Shen, J. Pan, and J. W. Mark, "Performance analysis of TCP-friendly AIMD algorithms for multimedia applications," *IEEE Transactions on Multimedia*, vol. 7, no. 2, pp. 339–355, 2005.

[49] L. Cai, X. Shen, and J. W. Mark, "Multimedia services in wireless Internet: modeling and analysis," 2009.

[50] J. Iyengar and M. Thomson, "QUIC: A udp-based multiplexed and secure transport," RFC 9000, May 2021. [Online]. Available: https://rfc-editor.org/rfc/rfc9000.txt

[51] J. Pan, J. Zhao, and L. Cai, "Measuring a low-earth-orbit satellite network," *2023 International Symposium on Personal, Indoor and Mobile Radio Communications*, 2023.

[52] Wikipedia, "Transponder (satellite communications)," 2023. [Online]. Available: https://en.wikipedia.org/wiki/Transponder_(satellite_communications)

[53] J. Xu, L. Wang, C. Song, D. Tang, and Z. Xu, "Toward bandwidth-efficient data distribution in satellite networks," in *Proceedings of the 2018 International Conference on Transportation & Logistics, Information & Communication, Smart City (TLICSC 2018)*. Atlantis Press, 2018/11, pp. 393–399. [Online]. Available: https://doi.org/10.2991/tlicsc-18.2018.63

[54] O. Popescu, "Power budgets for cubesat radios to support ground communications and inter-satellite links," *IEEE Access*, vol. 5, pp. 12 618–12 625, 2017.

[55] J. Huang, Y. Su, W. Liu, and F. Wang, "Adaptive modulation and coding techniques for global navigation satellite system inter-satellite communication based on the channel condition," *Iet Communications*, vol. 10, no. 16, pp. 2091–2095, 2016.

[56] R. E. Kalman, "A new approach to linear filtering and prediction problems," *Journal of Basic Engineering*, vol. 82, no. 1, pp. 35–45, 1960.

[57] M. R. Rajamani and J. B. Rawlings, "Estimation of the disturbance structure from data using semidefinite programming and optimal weighting," *Automatica*, vol. 45, no. 1, pp. 142–148, 2009.

[58] J. Deutschmann, K.-S. Hielscher, and R. German, "Satellite Internet performance measurements," in *2019 International Conference on Networked Systems (NetSys)*. IEEE, 2019, pp. 1–4.

[59] L. Yan, X. Fang, and Y. Fang, "A novel network architecture for C/U-plane staggered handover in 5G decoupled heterogeneous railway wireless systems," *IEEE Transactions on Intelligent Transportation Systems*, vol. 18, no. 12, pp. 3350–3362, 2017.

[60] M. A. Alrshah, M. A. Al-Maqri, and M. Othman, "Elastic-TCP: Flexible congestion control algorithm to adapt for high-BDP networks," *IEEE Systems Journal*, vol. 13, no. 2, pp. 1336–1346, 2019.
[61] Q. Peng, A. Walid, J. Hwang, and S. H. Low, "Multipath TCP: Analysis, design, and implementation," *IEEE/ACM Transactions on Networking*, vol. 24, no. 1, pp. 596–609, 2016.
[62] K. Gao, C. Xu, P. Zhang, J. Qin, L. Zhong, and G.-M. Muntean, "GCH-MV: Game-enhanced compensation handover scheme for multipath TCP in 6G software defined vehicular networks," *IEEE Transactions on Vehicular Technology*, vol. 69, no. 12, pp. 16 142–16 154, 2020.
[63] "quic-ns-3." [Online]. Available: https://github.com/signetlabdei/quic-ns-3
[64] M. Sandri, M. Pagin, M. Giordani, and M. Zorzi, "Implementation of a channel model for non-terrestrial networks in ns-3," *arXiv preprint arXiv:2305.05544*, 2023.
[65] O. B. Osoro and E. J. Oughton, "A techno-economic framework for satellite networks applied to low earth orbit constellations: Assessing Starlink, OneWeb and Kuiper," *IEEE Access*, vol. 9, pp. 141 611–141 625, 2021.
[66] I. Del Portillo, B. G. Cameron, and E. F. Crawley, "A technical comparison of three low earth orbit satellite constellation systems to provide global broadband," *Acta Astronautica*, vol. 159, pp. 123–135, 2019.

Wenjun Yang is currently a Ph.D. candidate in the Department of Electrical & Computer Engineering at the University of Victoria, British Columbia, Canada. His research interests include multipath QUIC/TCP, video streaming, deep reinforcement learning, and next generation of network architecture. He is a Graduate Student Member of IEEE.

Lin Cai (Fellow, IEEE) (S'00-M'06-SM'10-F'20) has been with the Department of Electrical & Computer Engineering at the University of Victoria since 2005 and is currently a Professor. She is an NSERC E.W.R. Steacie Memorial Fellow, a Canadian Academy of Engineering (CAE) Fellow, an Engineering Institute of Canada (EIC) Fellow, and an IEEE Fellow. In 2020, she was elected as a Member of the Royal Society of Canada's College of New Scholars, Artists and Scientists, and a 2020 "Star in Computer Networking and Communications" by N2Women. Her research interests span several areas in communications and networking, with a focus on network protocol and architecture design supporting ubiquitous intelligence. She received the NSERC Discovery Accelerator Supplement (DAS) Grants in 2010 and 2015, respectively. She cofounded and chaired the IEEE Victoria Section Vehicular Technology and Communications Joint Societies Chapter. She has been elected to serve the IEEE Vehicular Technology Society (VTS) Board of Governors, 2019 - 2024, and served as its VP Mobile Radio from 2023 to 2024. She served as a Board Member of IEEE Women in Engineering from 2022 to 2024, and a Board Member of IEEE Communications Society (ComSoc) from 2024 - 2026. She has held various editorial roles, including Associate Editor-in-Chief for IEEE Transactions on Vehicular Technology and membership in the Steering Committee of the IEEE Transactions on Mobile Computing (TMC), IEEE Transactions on Big Data (TBD), and IEEE Transactions on Cloud Computing (TCC). She has also been an Associate Editor of the IEEE/ACM Transactions on Networking, IEEE Internet of Things Journal, IEEE Transactions on Wireless Communications, IEEE Transactions on Vehicular Technology, IEEE Transactions on Communications. Lin Cai is a Distinguished Lecturer of the IEEE VTS and IEEE Communications Societies, and a registered professional engineer in British Columbia, Canada.

Shengjie Shu received the M.Sc. degree in Computer Science from University of Victoria, Victoria, BC, Canada in 2023. Her research interests include next generation of network architecture and related issues, such as multipath QUIC/TCP, AI for networking, and software development. She is a Student Member of IEEE.

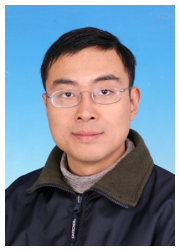

Jianping Pan is a professor of computer science at the University of Victoria, British Columbia, Canada. He received his Bachelor's and PhD degrees in computer science from Southeast University, Nanjing, Jiangsu, China, and he did his postdoctoral research at the University of Waterloo, Ontario, Canada. He also worked at Fujitsu Labs and NTT Labs. His area of specialization is computer networks and distributed systems, and his current research interests include protocols for advanced networking, performance analysis of networked systems, and applied network security. He received IEICE Best Paper Award in 2009, Telecommunications Advancement Foundation's Telesys Award in 2010, WCSP 2011 Best Paper Award, IEEE Globecom 2011 Best Paper Award, JSPS Invitation Fellowship in 2012, IEEE ICC 2013 Best Paper Award, NSERC DAS Award in 2016, IEEE ICDCS 2021 Best Poster Award and DND/NSERC DGS Award in 2021, and has been serving on the technical program committees of major computer communications and networking conferences including IEEE INFOCOM, ICC, Globecom, WCNC and CCNC. He was the Ad Hoc and Sensor Networking Symposium Co-Chair of IEEE Globecom 2012 and an Associate Editor of IEEE Transactions on Vehicular Technology. He is a senior member of the ACM and a Fellow of the IEEE.